Chemical Science

ROYAL SOCIETY OF CHEMISTRY

EDGE ARTICLE

View Article Online
View Journal | View Issue

Cite this: *Chem. Sci.*, 2020, **11**, 4131

All publication charges for this article have been paid for by the Royal Society of Chemistry

Received 10th March 2020
Accepted 1st April 2020

DOI: 10.1039/d0sc01459a

rsc.li/chemical-science

Diastereoselective olefin amidoacylation *via* photoredox PCET/nickel-dual catalysis: reaction scope and mechanistic insights†

Shuai Zheng, [a] Shuo-Qing Zhang, [b] Borna Saeednia, [a] Jiawang Zhou, [a] Jessica M. Anna, [a] Xin Hong *[b] and Gary A. Molander *[a]

The selective 1,2-aminoacylation of olefins provides opportunities for the rapid construction of nitrogen-containing molecules. However, the lack of CO-free acylation reactions has limited their application. By using photoredox proton-coupled electron transfer (PCET)/Ni dual-catalysis, a highly regio- and diastereoselective amidoacylation of unactivated olefins has been developed. Various acyl electrophiles are compatible, including alkyl- and aryl acyl chlorides and anhydrides, as well as *in situ* activated carboxylic acids. Hammett studies and other mechanistic experiments to elucidate features of the diastereoselectivity, a transient absorption study of the PCET step, as well as computational evidence, provide an in-depth understanding of the disclosed transformation.

Introduction

Transition-metal catalyzed 1,2-difunctionalizations of unactivated olefins have emerged as powerful methods for the elaboration of commodity chemicals over the past decades, with attractive capabilities for rapidly building molecular complexity.[1–5] Multiple strategies have been employed to achieve selectivity in the heterodifunctionalization, such as directed migratory insertion,[6] nucleometalation,[7] radical-polar crossover of activated olefins,[8] utilization of bulky coupling partners and/or polarity reversal,[9–13] as well as kinetically favorable radical cyclization approaches.[14,15] Among these transformations, carboamination has received significant attention because of the prevalence of nitrogen-containing small molecules and heterocycles in bio-active and drug-like molecules.[16] Progress has been achieved using amines as nucleophilic species for directed aminopalladation[6,17] or trapping of cationic species after C–C bond formation.[8,18] Efforts have also been made to utilize prefunctionalized, reductively generated amidyl- and iminyl radicals[19–21] to improve efficiency and selectivity, while the oxidative proton-coupled electron transfer (PCET) approach has been utilized to generate *N*-centered radicals directly from N–H functional units.[14,15,22–25]

Although β-amino ketone structures are reasonably prevalent among bioactive molecules (Fig. 1A), aminoacylation reactions and aminocarbonylative transformations of olefins appear relatively rare (Fig. 1B). Early efforts were focused on net-oxidative transformations, rendering β-amino esters as the final product,[26,27] while the Lambert group accessed amidoacylation products by tethering a Pd-catalyzed carbonylation process with a Lewis acid-catalyzed Friedel–Crafts acylation of electron-rich (hetero)aromatic systems.[28] Later, others utilized an Umpolung approach using a tethered oxime ester as an electrophilic nitrogen source and disclosed iminoacylation transformations using tetraaryl borates or organozinc reagents.[29,30] In a more recent report,[31] such transformations were achieved with aryl iodides using an 8-aminoquinoline directing group.

Together, these approaches provide a powerful suite of methods for the synthesis of *N*-heterocycles as well as β-amino ketone structures, yet many challenges remain to be addressed. One common feature of these transformations is the need for CO gas, which, although inexpensive and abundant, is toxic and flammable. Additionally, the majority of present transformations require aryl electrophiles or nucleophiles, while alkyl electrophiles remain challenging to incorporate. Because of their good commercial availability and convenient preparation, acyl (pseudo)halides are useful surrogates to consider in such transformations.[32]

As attractive as the utilization of *N*-centered radicals might be,[20,33–35] the application of such intermediates in transition metal catalysis still remains rare (Fig. 1C). Apart from several reports facilitating direct C–N bond construction,[36] transition metal-catalyzed cascade transformations, where *C*-centered radicals were generated *via* either 1,5-HAT[37,38] or 5-*exo*-trig

[a]*Roy and Diana Vagelos Laboratories, Department of Chemistry, University of Pennsylvania, 231 South 34th Street, Philadelphia, Pennsylvania 19104-6323, USA. E-mail: gmolandr@sas.upenn.edu*

[b]*Department of Chemistry, Zhejiang University, Hangzhou, Zhejiang 310027, China*

† Electronic supplementary information (ESI) available. CCDC 1981876. For ESI and crystallographic data in CIF or other electronic format see DOI: 10.1039/d0sc01459a

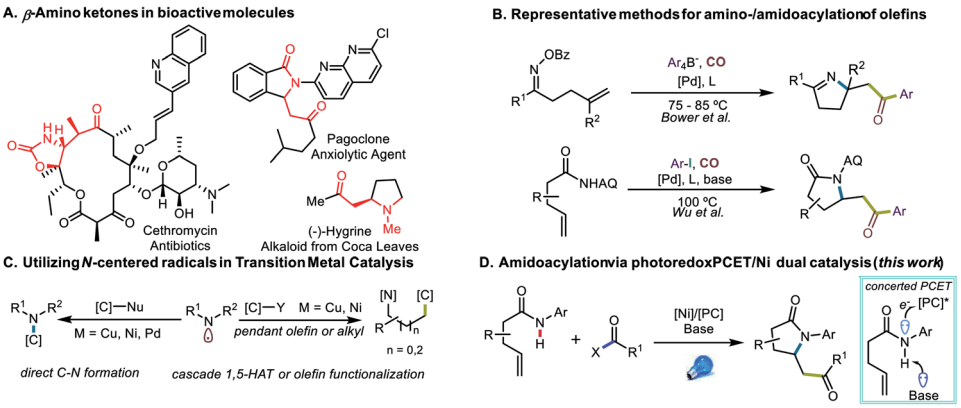

Fig. 1 Amidoacylation of olefin species.

cyclization,[15,20] to this point are scarce, possibly because of potential selectivity issues and the incompatibility between transition metal catalysts and *N*-radical generation. Therefore, inspired by our recent efforts to meld photoredox PCET with nickel catalysis for amidoarylation of olefins,[15] we sought to address the challenges of amidoacylation by utilizing acyl electrophiles in photoredox PCET/Ni dual-catalyzed olefin difunctionalization (Fig. 1D).

Results and discussion

To test this strategy, an investigation was initiated using *N*-phenyl hex-4-enamide and benzoyl chloride as cross-coupling partners (Scheme 1). Previous reports pointed to 1,2-dichloroethane (DCE) as a potential solvent for photoredox PCET/Ni dual catalysis,[15] which indeed rendered a 46% yield in the initial attempt (Scheme 1, entry 1). Although it is noteworthy that the less expensive organic photocatalyst 4CzIPN gave a comparable yield (entry 3), neither this nor a more oxidizing Ir photocatalyst (**[Ir-2]**, entry 2) significantly improved the yield. Several ligands successfully promoted the reaction, with the electron-rich dMeObpy being most appropriate (entries 1, 4, 5). A careful examination of the reaction profile indicated a significant amount of hydroamidation byproduct, likely caused by hydrogen atom abstraction from the solvent,[23] which led us to a further solvent optimization. Acetonitrile was eventually identified as the most suitable solvent, rendering a 75% yield of **1** (entry 7). Owing to the vast availability of carboxylic acid functional groups in a variety of commodity chemicals, we also examined the possibilities of employing *in situ* activation of carboxylic acids as the source of the acyl electrophile.[39] After several attempts (entries 8–11), oxalyl chloride was identified as an appropriate activator, affording a 73% yield.

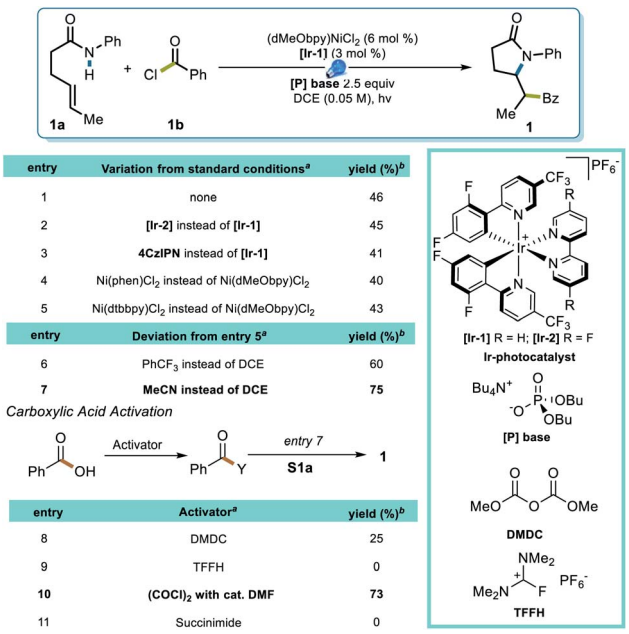

entry	Variation from standard conditions[a]	yield (%)[b]
1	none	46
2	**[Ir-2]** instead of **[Ir-1]**	45
3	**4CzIPN** instead of **[Ir-1]**	41
4	$Ni(phen)Cl_2$ instead of $Ni(dMeObpy)Cl_2$	40
5	$Ni(dtbbpy)Cl_2$ instead of $Ni(dMeObpy)Cl_2$	43
entry	**Deviation from entry 5[a]**	**yield (%)[b]**
6	$PhCF_3$ instead of DCE	60
7	**MeCN instead of DCE**	**75**

entry	Activator[a]	yield (%)[b]
8	DMDC	25
9	TFFH	0
10	**$(COCl)_2$ with cat. DMF**	**73**
11	Succinimide	0

Scheme 1 Reaction Optimization. [a]Performed on 0.1 mmol scale. [b]Isolated yield.

With proper conditions in hand, an exploration of the scope of the reaction was initiated. The developed reaction conditions allowed excellent functional group tolerance. For substituted benzoyl chlorides, electron-rich, electron-neutral, and electron-poor substrates all rendered reasonably good yields (Scheme 2, entries **1**–**7**). Interestingly, even though the terminal methyl group on the alkene seemed rather sterically undemanding, exceptional diastereoselectivities were observed in all of these examples. Other types of electrophiles, such as acyl anhydrides (**8**) and alkyl acyl halides (**9**–**11**), are also compatible, despite leading to a lower diastereoselectivity in some cases. Perhaps most importantly, *in situ* activation of carboxylic acids did not lead to a compromise in either the yield or dr of the reactions (**12**, **13**), and interesting substructures, such as substituted cyclopropyl (**14**) and difluorobenzodioxolyl (**15**), were installed with reasonable yields directly from the corresponding carboxylic acids.

Various anilide- and alkenyl backbones were next examined, and their influence in this reaction was tested both to expand the scope and to shed light on the diastereoselectivity. For aniline derivatives bearing different substituents (**16**–**22**), although the yields varied, the diastereoselectivities, where relevant, remained consistent. Substrates leading to primary

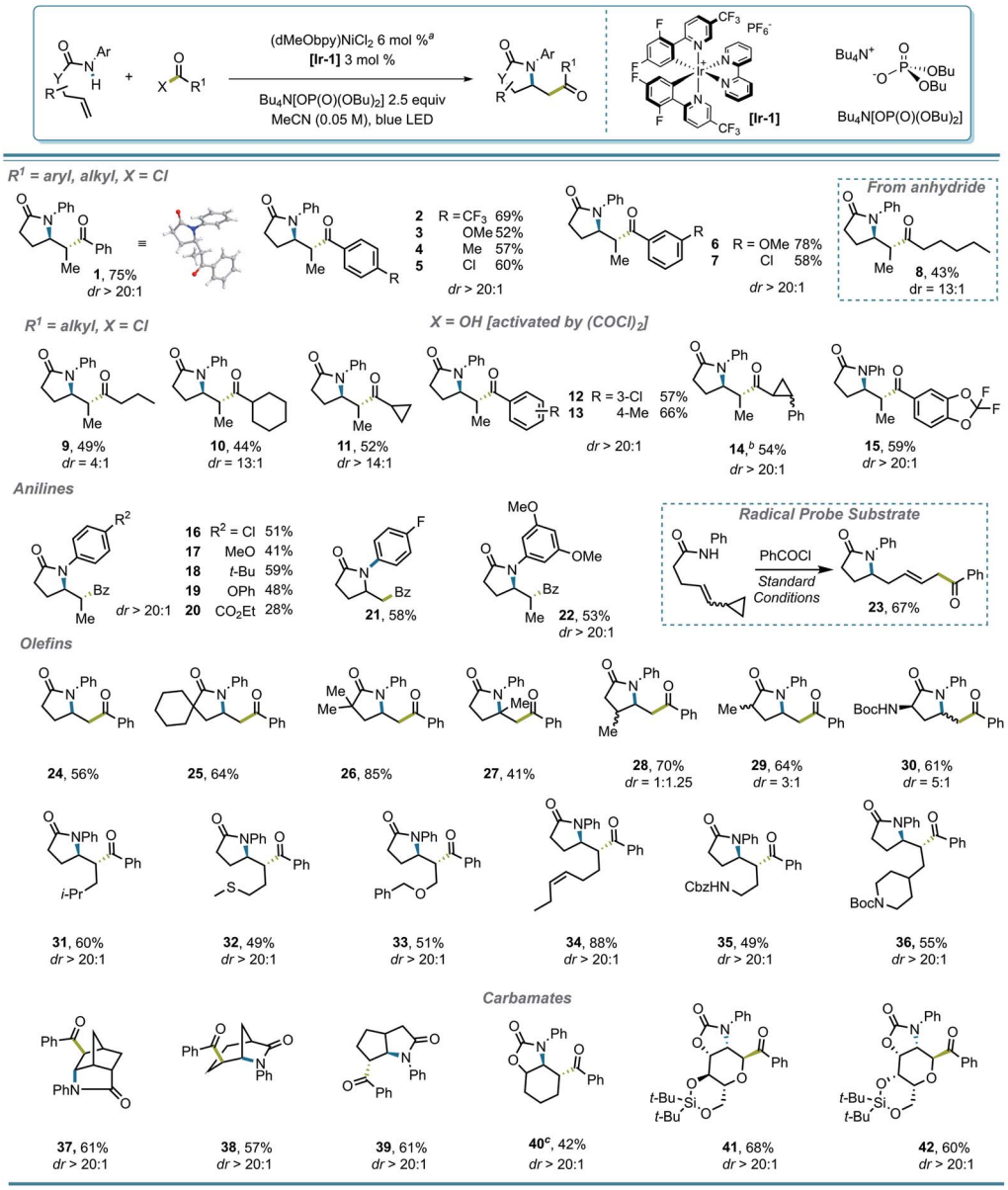

Scheme 2 Reaction scope. [a]Reaction conditions: amide **S1–S42** (0.36 mmol, 1.2 equiv.), acyl (pseudo)halides (0.3 mmol, 1.0 equiv.), $Bu_4N[OP(O)(OBu)_2]$ (0.75 mmol, 2.5 equiv.), $Ni(dMeObpy)Cl_2$ (0.018 mmol, 6 mol%), **[Ir-1]** (0.009 mmol, 3 mol%), blue LED, 6 mL MeCN. [b]A 1 : 1 mixture of two diastereoisomers originating from the acyl coupling partner. [c]0.006 mmol, 2 mol% of Ni precatalyst was used.

alkyl radicals were generally compatible in the reaction (**21**, **24–30**), and although both methyl and a bulky Boc-protected amino group at the α-carbonyl position induced diastereoselectivity to some extent (**29**, **30**), substitution β to the carbonyl seemed to have minimal influence (**28**). Therefore, it seems that substitution δ to the carbonyl, where the alkyl radical is generated after cyclization, is crucial for the high diastereoselectivity observed. Not surprisingly, polycyclic structures retain their high diastereoselectivity in the reaction (**37–39**).

Several functional groups were incorporated to test compatibility, including thioether (**32**), ether (**33**), and pendant olefin (**34**) groups, as well as protected primary- (**35**) and secondary (**36**) amines, all showing excellent dr and good to excellent yields. The applicability of the protocol for amidoacylation of alkenyl carbamates was also examined, which initially led to a diminished yield (20%) of **40**, with 35% of *N*-phenyl benzamide byproduct. This byproduct likely results from an S_N2'-type oxidative addition by the Ni(0) catalyst to the ene carbamate,[40] with loss of CO_2 and capture of the resulting aniline with the acid chloride. Lowering the loading of Ni precatalyst to 2% improved the yield of **40** to 42%. Interestingly, under standard reaction conditions, such a side reaction was not observed in monosaccharide-derived substrates (**41**, **42**), rendering *C*-acyl aminoglycosides diastereoselectively in good yields.

Several experiments were performed to aid in deciphering the mechanism of the reaction. First, control experiments suggested that nickel, Ir photocatalyst, light, and base are all

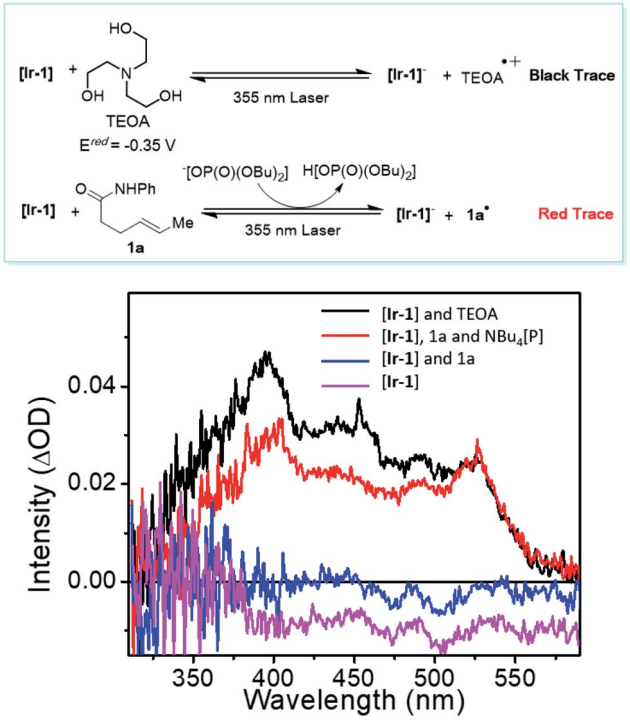

Fig. 2 Transient absorption studies on PCET-mediated *N*-radical generation at 10 μs time delay.

essential for the transformation (see ESI† for further details). Radical probe substrate **23** supported the proposed reaction pathway and indicated that the reaction indeed underwent a single electron transfer process. To rule out the possibility of energy transfer mechanism as seen in related systems,[41] we performed a transient absorption spectroscopy study of the PCET step (Fig. 2). By comparing the well-studied triethanolamine (TEOA) system (black trace, Fig. 2), which is known to reduce the excited state of the Ir photocatalyst,[42,43] with substrate **1a** in the presence of base [$Bu_4N[OP(O)(OBu)_2]$] (red trace, Fig. 2), the resulting spectrum suggested an evident generation of reduced **[Ir-1]** photocatalyst, supporting the proposed electron transfer mechanism, generating an *N*-centered radical. Then, considering the versatility of different electrophilic species, the nature of the actual electrophile in the reaction was sought. After stirring a 1 : 1 mixture of benzoyl chloride and $Bu_4N[OP(O)(OBu)_2]$ in CH_2Cl_2 for 20 min, the mixed benzoic-phosphonic anhydride was isolated and subjected to the reaction conditions, rendering a 73% yield and a comparable diastereoselectivity to that observed under the normal reaction conditions (Scheme 3a). Further computational studies also provide support that, compared to benzoyl chloride, the benzoic-phosphonic anhydride appears to be a more stable species (see ESI† for further details). Interestingly, a diminished yield was observed when an alkyl acyl chloride was used under the same protocol.

The origin of the high diastereoselectivity of this reaction was next explored. To investigate the stability of both stereoisomers, a synthesis of the opposite diastereoisomer was carried out. Thus, by applying the hydroamination reaction developed by Knowles *et al.*,[23] the designed substrate **S1′** led to diastereoisomer **1′**. This isomer was subsequently subjected to the standard reaction conditions, and no isomerization to **1** was observed (Scheme 3b). Further investigation revealed a dependence between the electron density on the ligands and the dr values (Scheme 3b). When an analysis was performed relating log dr to σ+ parameters,[44] a good linear correlation was found. The negative ρ value from this plot indicated that higher electron density on the ligand, which stabilizes the putative Ni(III) intermediates in the catalytic cycle, will lead to a higher diastereoselectivity in this transformation. Taken together, these results suggested that the high dr must originate from the catalytic process and not epimerization after product formation.[45]

To gain deeper insights on the diastereo-determining step, the investigation was continued using computational tools. First, the free energy calculation of **1** and **1′** indicated that **1′** is

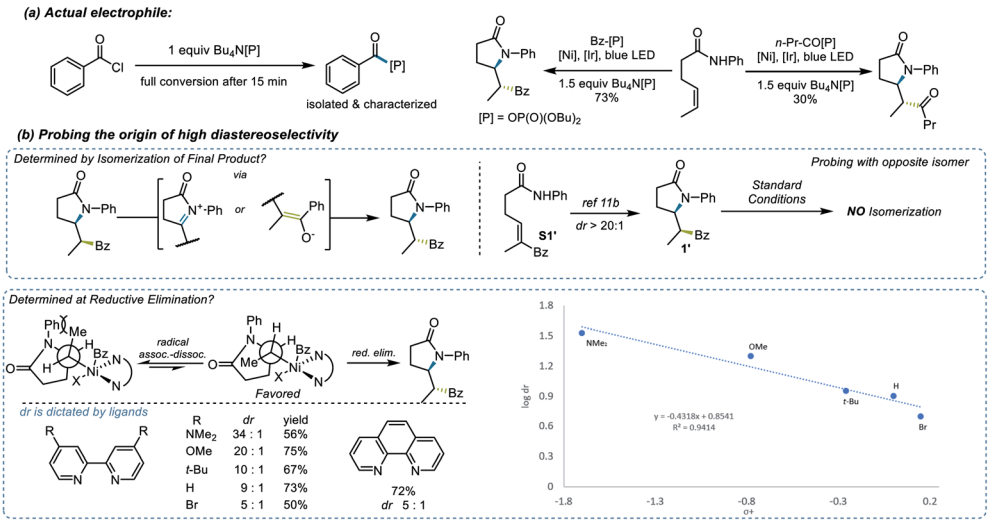

Scheme 3 Experimental mechanistic insights.

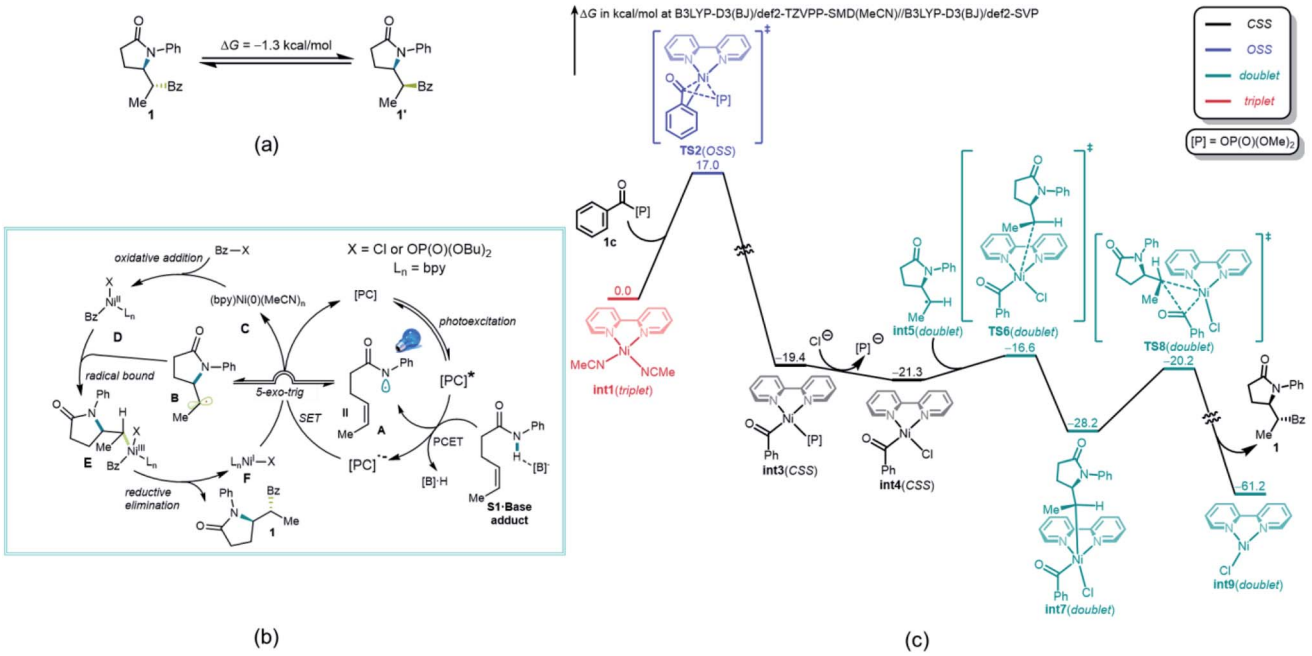

Fig. 3 (a) Free energy difference between **1** and **1′**. (b) Proposed reaction mechanism of the acylation between **1a** and **1b**. (c) DFT computed free energy diagram between **1a** and **1c** of the thermochemical part (from **C** to **F**) of the catalytic cycle calculated at B3LYP-D3(BJ)/def2-TZVPP-SMD(MeCN)//B3LYP-D3(BJ)/def2-SVP.

the thermodynamically more favorable isomer (Fig. 3a). Therefore, the diastereoselective formation of **1** is a kinetically controlled process. Although either a Ni(0)–Ni(I)–Ni(III) mechanism,[46] where radical addition takes place before oxidative addition of acyl halide, or a Ni(0)–Ni(II)–Ni(III) mechanism appear viable, because Bz–X is in much higher concentration than the photogenerated radicals **A** and **B**, the major reaction pathway proposed is one in which oxidative addition of Bz–X to a catalytically active nickel complex that initiates the process. Regardless of the mechanistic pathway, the diastereo-determining step will be the addition of radical **B** to nickel complex **D** (*vide infra*). Thus, Ni(0) catalyst **C** first undergoes oxidative addition to Bz–X, forming Ni(II) species **D**, which subsequently binds the radical **B** generated through a kinetically favorable 5-*exo*-trig cyclization.[46] The formed Ni(III) species **E** then undergoes reductive elimination, releasing product **1** and generating Ni(I) species **F**. Further SET between **F** and reduced photocatalyst $[PC]^{\bullet-}$ regenerates active Ni(0) catalyst **C**.

Based on the proposed reaction mechanism in Fig. 3b, the most favorable computed free energy pathway for the thermochemical part (**B** to **F**) of the catalytic cycle calculated by density functional theory (DFT) is shown in Fig. 3c. Although both BzCl and Bz-[P] (**1c**) exhibited reasonable reactivity toward oxidative addition, the mixed anhydride Bz-[P] was applied as the initial point because of its greater stability and ease of formation (see ESI† for further details). The active triplet Ni(0) catalyst **int1** is oxidized by Bz-[P] (**1c**) *via* an open-shell singlet (OSS) transition state **TS2**, which is quite facile, with a free energy barrier of only 17.0 kcal mol^{-1}. This generates closed-shell Ni(II) species **int3**. This step is strongly exothermic and thus irreversible as proposed. Ligand exchange between the Cl^- anion and the $[P]^-$ anion then generates a more stable Ni(II) species **int4**. The subsequent radical binding step between **int4** and **int5** *via* **TS6** is also very fast, with a free energy barrier of only 4.7 kcal mol^{-1}, generating doublet Ni(III) species **int7**. Further irreversible and highly exothermic reductive elimination *via* **TS8** possesses a free energy barrier of 8.0 kcal mol^{-1}, generating product **1** and doublet Ni(I) species **int9**.

Somewhat surprisingly, **TS6** is calculated to be 3.6 kcal mol^{-1} higher in energy than **TS8**, and conversion of **int7** through **TS8** is fast and irreversible. Thus, it is the radical binding step *via* **TS6** that determines the observed diastereoselectivity. As shown in Fig. 4, **TS10**, which leads to the diastereomeric product **1′**, is 1.0 kcal mol^{-1} higher in energy than **TS6**, which is in good agreement with the observed dr of 9 : 1 using bpy as ligand. The highlighted steric issues between the Me and Ph groups elevate

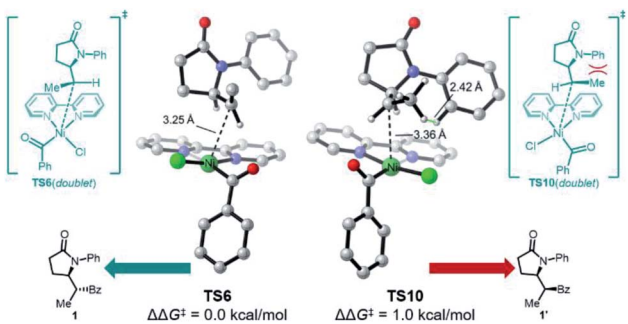

Fig. 4 3D renderings of diastereoselectivity-determining radical bound transition states **TS5** and **TS9** calculated at B3LYP-D3(BJ)/def2-TZVPP-SMD(MeCN)//B3LYP-D3(BJ)/def2-SVP. Trivial H atoms are omitted for clarity.

the free energy **TS10** and is responsible for the observed diastereoselectivity.

Conclusions

In conclusion, we have disclosed a photoredox PCET/Ni dual-catalyzed diastereoselective amidoacylation of unfunctionalized olefins. Various acyl electrophiles, including alkyl- and aryl acyl chlorides and anhydrides, as well as carboxylic acids activated *in situ*, are incorporated and retain excellent dr values in most of the examples. Thanks to the mild conditions, various functional groups, such as thioethers, protected amines, and saccharide derivatives are compatible. Transient spectroscopy provides strong support for electron transfer between the amide substrates and the Ir photocatalyst in the presence of phosphate base. Other mechanistic experiments indicate that the diastereoselectivity originates in the Ni-catalytic cycle, while the Hammett plot as well as a detailed computational study provide insight into the electronic and steric effects that lead to the diastereo-determining step toward the kinetic product. This study not only provides a powerful tool toward olefin hetero-difunctionalization, but also sheds light on future reaction development.

Conflicts of interest

There are no conflicts to declare.

Acknowledgements

The authors are grateful for the financial support provided by NIGMS (R35 GM 131680 to G. A. M.). We thank Dr Charles W. Ross, III (University of Pennsylvania) for obtaining HRMS data. We gratefully acknowledge Dr Mike Gau and Dr Pat Carroll (University of Pennsylvania) for acquiring X-ray crystal structures. We thank Dr Alvaro Gutierrez-Bonet (Merck & Co.) and Prof. Marisa C. Kozlowski (University of Pennsylvania) for helpful discussions. We acknowledge Johnson-Matthey for fine chemicals donations. Financial support from the NSFC (21702182 and 21873081 to X. H.), "Fundamental Research Funds for the Central Universities" (2019QNA3009 to X. H.) and China Postdoctoral Science Foundation (2018M640546 to S.-Q. Z.) is gratefully acknowledged. Calculations were performed on the high-performance computing system at the Department of Chemistry, Zhejiang University.

Notes and references

1 M.-Y. Cao, X. Ren and Z. Lu, *Tetrahedron Lett.*, 2015, **56**, 3732–3742.
2 X.-W. Lin, N.-X. Wang and Y. Xing, *Eur. J. Org. Chem.*, 2017, 5821–5851.
3 H.-M. Huang, M. H. Garduño-Castro, C. Morrill and D. J. Procter, *Chem. Soc. Rev.*, 2019, **48**, 4626–4638.
4 J. Derosa, V. T. Tran, V. A. van der Puyl and K. M. Engle, *Aldrichimica Acta*, 2018, **51**, 21–32.
5 R. K. Dhungana, S. KC, P. Basnet and R. Giri, *Chem. Rec.*, 2018, **18**, 1314–1340.
6 J. E. Ney and J. P. Wolfe, *Angew. Chem., Int. Ed.*, 2004, **43**, 3605–3608.
7 R. I. McDonald, G. Liu and S. S. Stahl, *Chem. Rev.*, 2011, **111**, 2981–3019.
8 G. Fumagalli, S. Boyd and M. F. Greaney, *Org. Lett.*, 2013, **15**, 4398–4401.
9 M. W. Campbell, J. S. Compton, C. B. Kelly and G. A. Molander, *J. Am. Chem. Soc.*, 2019, **141**, 20069–20078.
10 A. García-Domínguez, R. Mondal and C. Nevado, *Angew. Chem., Int. Ed.*, 2019, **58**, 12286–12290.
11 W. Shu, A. García-Domínguez, M. T. Quirós, R. Mondal, D. J. Cárdenas and C. Nevado, *J. Am. Chem. Soc.*, 2019, **141**, 13812–13821.
12 S. W. Lardy and V. A. Schmidt, *Eur. J. Org. Chem.*, 2019, 6796–6799.
13 J. M. Lear, J. Q. Buquoi, X. Gu, K. Pan, D. N. Mustafa and D. A. Nagib, *Chem. Commun.*, 2019, **55**, 8820–8823.
14 G. J. Choi and R. R. Knowles, *J. Am. Chem. Soc.*, 2015, **137**, 9226–9229.
15 S. Zheng, Á. Gutiérrez-Bonet and G. A. Molander, *Chem*, 2019, **5**, 339–352.
16 E. Vitaku, D. T. Smith and J. T. Njardarson, *J. Med. Chem.*, 2014, **57**, 10257–10274.
17 Z. Liu, Y. Wang, Z. Wang, T. Zeng, P. Liu and K. M. Engle, *J. Am. Chem. Soc.*, 2017, **139**, 11261–11270.
18 B. Sahoo, M. N. Hopkinson and F. Glorius, *J. Am. Chem. Soc.*, 2013, **135**, 5505–5508.
19 J. Davies, N. S. Sheikh and D. Leonori, *Angew. Chem., Int. Ed.*, 2017, **56**, 13361–13365.
20 L. Angelini, J. Davies, M. Simonetti, L. M. Sanz, N. S. Sheikh and D. Leonori, *Angew. Chem., Int. Ed.*, 2019, **58**, 5003–5007.
21 K. M. Nakafuku, S. C. Fosu and D. A. Nagib, *J. Am. Chem. Soc.*, 2018, **140**, 11202–11205.
22 A. J. Musacchio, L. Q. Nguyen, G. H. Beard and R. R. Knowles, *J. Am. Chem. Soc.*, 2014, **136**, 12217–12220.
23 D. C. Miller, G. J. Choi, H. S. Orbe and R. R. Knowles, *J. Am. Chem. Soc.*, 2015, **137**, 13492–13495.
24 G. J. Choi, Q. Zhu, D. C. Miller, C. J. Gu and R. R. Knowles, *Nature*, 2016, **539**, 268.
25 J. C. K. Chu and T. Rovis, *Nature*, 2016, **539**, 272.
26 L. S. Hegedus, G. F. Allen and D. J. Olsen, *J. Am. Chem. Soc.*, 1980, **102**, 3583–3587.
27 L. S. Hegedus, P. M. Winton and S. Varaprath, *J. Org. Chem.*, 1981, **46**, 2215–2221.
28 T. A. Cernak and T. H. Lambert, *J. Am. Chem. Soc.*, 2009, **131**, 3124–3125.
29 A. Faulkner, J. S. Scott and J. F. Bower, *J. Am. Chem. Soc.*, 2015, **137**, 7224–7230.
30 L. M. Ambrosini, T. A. Cernak and T. H. Lambert, *Synthesis*, 2010, **2010**, 870–881.
31 J.-B. Peng, F.-P. Wu, D. Li, H.-Q. Geng, X. Qi, J. Ying and X.-F. Wu, *ACS Catal.*, 2019, **9**, 2977–2983.
32 L. Wang and C. Wang, *Org. Chem. Front.*, 2018, **5**, 3476–3482.
33 J.-R. Chen, X.-Q. Hu, L.-Q. Lu and W.-J. Xiao, *Chem. Soc. Rev.*, 2016, **45**, 2044–2056.

34 G. B. Boursalian, M.-Y. Ngai, K. N. Hojczyk and T. Ritter, *J. Am. Chem. Soc.*, 2013, **135**, 13278–13281.
35 T. Xiong and Q. Zhang, *Chem. Soc. Rev.*, 2016, **45**, 3069–3087.
36 L. Zhou, S. Tang, X. Qi, C. Lin, K. Liu, C. Liu, Y. Lan and A. Lei, *Org. Lett.*, 2014, **16**, 3404–3407.
37 Z. Zhang, L. M. Stateman and D. A. Nagib, *Chem. Sci.*, 2019, **10**, 1207–1211.
38 S. M. Thullen, S. M. Treacy and T. Rovis, *J. Am. Chem. Soc.*, 2019, **141**, 14062–14067.
39 J. Amani and G. A. Molander, *Org. Lett.*, 2017, **19**, 3612–3615.
40 A. Agarkov, E. W. Uffman and S. R. Gilbertson, *Org. Lett.*, 2003, **5**, 2091–2094.
41 T. Kim, S. J. McCarver, C. Lee and D. W. C. MacMillan, *Angew. Chem., Int. Ed.*, 2018, **57**, 3488–3492.
42 A. Paul, M. D. Smith and A. K. Vannucci, *J. Org. Chem.*, 2017, **82**, 1996–2003.
43 C.-F. Leung, S.-M. Ng, C.-C. Ko, W.-L. Man, J. Wu, L. Chen and T.-C. Lau, *Energy Environ. Sci.*, 2012, **5**, 7903–7907.
44 C. Hansch, A. Leo and R. W. Taft, *Chem. Rev.*, 1991, **91**, 165–195.
45 N. Y. Shin, J. M. Ryss, X. Zhang, S. J. Miller and R. R. Knowles, *Science*, 2019, **366**, 364–369.
46 See ESI† for details. For references, see: (*a*) O. Gutierrez, J. C. Tellis, D. N. Primer, G. A. Molander and M. C. Kozlowski, *J. Am. Chem. Soc.*, 2015, **137**, 4896–4899; (*b*) E. Martinez and M. Newcomb, *J. Org. Chem.*, 2006, **71**, 557–561.